

## Diagnosis of Interaction-driven Topological Phase via Exact Diagonalization

Han-Qing Wu,<sup>1</sup> Yuan-Yao He,<sup>1</sup> Chen Fang,<sup>2,\*</sup> Zi Yang Meng,<sup>2,†</sup> and Zhong-Yi Lu<sup>1</sup>

<sup>1</sup>Department of Physics, Renmin University of China, Beijing 100872, China

<sup>2</sup>Beijing National Laboratory for Condensed Matter Physics, and Institute of Physics, Chinese Academy of Sciences, Beijing 100190, China

(Received 18 February 2016; published 5 August 2016)

We propose a general scheme for diagnosing interaction-driven topological phases in the weak interaction regime using exact diagonalization (ED). The scheme comprises the analysis of eigenvalues of the point-group operators for the many-body eigenstates and the correlation functions for physical observables to extract the symmetries of the order parameters and the topological numbers of the underlying ground states at the thermodynamic limit from a relatively small size system afforded by ED. As a concrete example, we investigate the interaction effects on the half-filled spinless fermions on the checkerboard lattice with a quadratic band crossing point. Numerical results support the existence of a spontaneous quantum anomalous Hall phase purely driven by a nearest-neighbor weak repulsive interaction, separated from a nematic Mott insulator phase at strong repulsive interaction by a first-order phase transition.

DOI: 10.1103/PhysRevLett.117.066403

*Introduction.*—The pursuit of interaction-driven topological phases in fermions is becoming a collective activity in the condensed matter physics community [1–18], as people are expecting that such phases, if discovered, will combine both the richness of many-body effects and the elegance of topological physics. In Ref. [19], Raghu and co-workers proposed the possibility of repulsive interaction generated current loops (spin-orbital coupling) in spinless (spin-1/2) electrons on a honeycomb lattice, which gives rise to quantum anomalous Hall (QAH) [quantum spin Hall (QSH)] phases. Although more recent analytical and numerical works [12,20–28] have disputed the proposal in that particular model, alternative routes towards the realization of interaction-driven topological phases are currently being actively explored [14,15,18,29–38].

On the other hand, in a 2D system, unlike the Dirac point, a quadratic band crossing point (QBCP) with finite density of states (DOS) at the Fermi energy is unstable for arbitrarily weak interactions, leading to the possibility of spontaneous breaking of rotational symmetry (nematic phase) or time-reversal invariance [11,39–44]. In Ref. [42], Sun and co-workers proposed that the short-range repulsive interaction in spinless fermions is marginally relevant in a one-loop renormalization group, and the leading mean-field instability is towards a QAH insulator with broken time-reversal symmetry. At the noninteracting limit, the QBCP acquires a dynamic critical exponent  $z = 2$ , which renders the effective dimension of the underlying 2D system 4, and, hence, the corresponding mean-field analysis is likely to be permitted by the Ginzburg criterion [45].

To diagnose the interaction-driven topological phases, in this work, we design a scheme that enables us to extract

definitive information on the thermodynamic ground state, including the symmetries of the phases and their topological numbers, from relatively small size systems studied by ED. Such a diagnosis scheme is comprised of the analyses of eigenvalues of the point-group operators for the many-body eigenstates and the correlation functions for physical observables. We apply this scheme to the half-filled spinless fermions on the checkerboard lattice with a quadratic band crossing point [46]. We map out the full phase diagram in the parameter space with two gapped phases: a time-reversal breaking QAH phase at small repulsive interaction and a rotation symmetry breaking site-nematic Mott insulator (NMI) phase at large repulsive interaction, which are separated by a first-order quantum phase transition. This is the first time that the eigenvalues of the many-body eigenstates are used to infer the topological numbers in ED, and we remark that a similar method can be used to diagnose other topological phases in the weak interaction regime, such as the quantum spin Hall state and the  $p + ip$  superconducting state.

*Model and method.*—The system studied in this Letter has the following Hamiltonian,

$$\hat{H} = -\sum_{ij}(t_{ij}\hat{c}_i^\dagger\hat{c}_j + \text{H.c.}) + \mu\sum_i\hat{n}_i + V\sum_{\langle ij\rangle}\hat{n}_i\hat{n}_j, \quad (1)$$

where  $t_{ij}$  is the hopping amplitude between sites  $i$  and  $j$ , and  $V$  is the nearest-neighbor repulsion. As shown in Fig. 1(a),  $t_{ij} = t, t', t''$ , respectively, standing for the nearest ( $t$ , black solid lines), one type of next-nearest ( $t'$ , purple long-dashed lines) and the other type of next-nearest ( $t''$ , yellow short-dashed lines) neighbor hopping amplitudes. We set  $t' = -t''$  to achieve the particle-hole symmetry (although our results also hold for the non-particle-hole

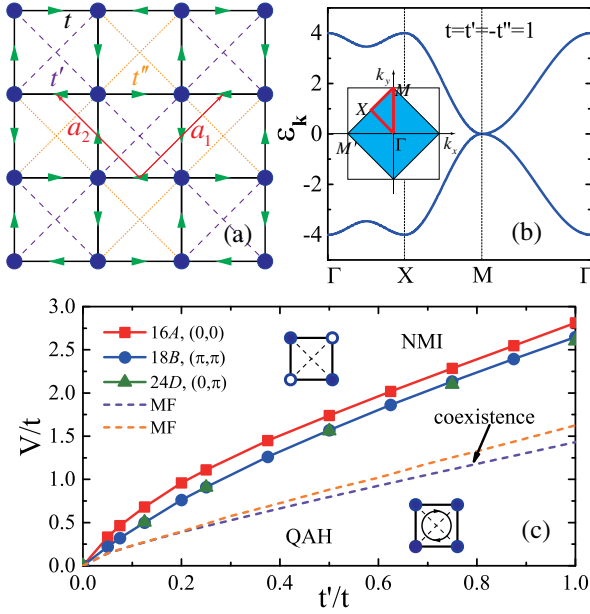


FIG. 1. (a) 16A cluster of the checkerboard lattice. Two next-nearest-neighbor hopping amplitudes  $t'$  and  $t''$  are differentiated by the purple long-dashed and orange short-dashed lines. The green arrows represent the current loops in the spontaneous QAH phase.  $\mathbf{a}_1 = (1, 1)$ ,  $\mathbf{a}_2 = (-1, 1)$  are the primitive vectors. (b) Noninteracting band structure along the high-symmetry path  $\Gamma(0, 0) \rightarrow X(\pi/2, \pi/2) \rightarrow M(0, \pi) \rightarrow \Gamma(0, 0)$ . Unlike the massless Dirac points in honeycomb lattice, the QBCP gives rise to a finite DOS. (c) The ground state phase diagram obtained from ED calculations. We use the level crossing (avoided level crossing) in the 16A (18B, 24D) cluster under the periodic [antiperiodic,  $(0, \pi)$  twisted phase] boundary condition to determine the phase boundary. Phase boundaries determined from self-consistent mean-field calculation are also presented with dashed lines. Insets are the caricatures of the QAH and NMI order parameters in real space.

symmetric case) and set chemical potential  $\mu = -2V$  to guarantee half-filling [41,42]. To simplify the notation, the nearest-neighbor hopping  $t$  and the nearest-neighbor bond length  $a$  are set to be units of energy and length.

The model in Eq. (1) acquires  $C_4$  point-group symmetry and time-reversal symmetry  $T$ . The QBCP at the  $M$  point [shown in Fig. 1(b)] with monopole flux  $2\pi$  in the noninteracting band structure is protected by the combined symmetry of  $T$  and  $C_4$  [40–42,50]. In the ED calculations, we employed clusters with four different geometries (denoted as 16A, 18B, 24C, and 24D, as shown in the Sec. I of the Supplemental Material [51]). The results in the main text, especially the analysis of eigenvalues of the  $C_4$  operators, are mainly obtained from the 16A cluster which respects the full symmetries of the Hamiltonian. Some physical observables of other clusters, particularly the 18B cluster which also respects the  $C_4$  symmetry, are also presented. For a given cluster, we apply a chosen set of twisted phases at the boundaries to ensure that the QBCP is included at the discretized single-particle momenta.

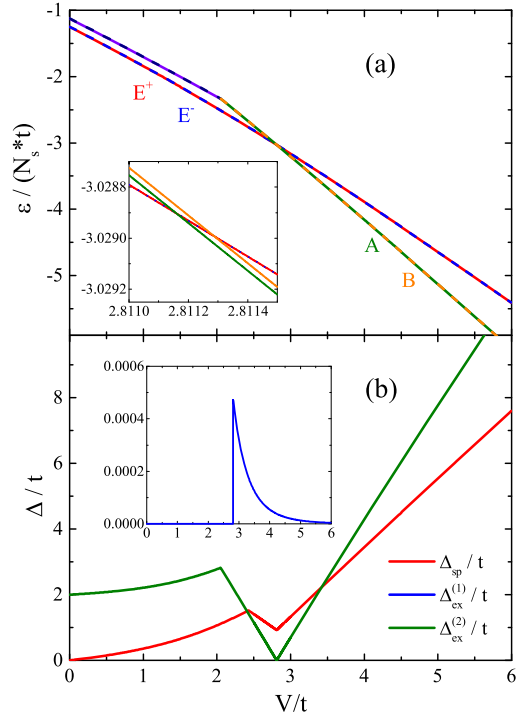


FIG. 2. (a) Energy density of the four lowest energy levels in the 16A as a function of  $V/t$ . The inset is an enlargement of the level crossing close to  $V_c \approx 2.81t$ .  $E^\pm$ ,  $A$ , and  $B$  label the four energy levels with their corresponding  $C_4$  representation. (b) Single-particle gap  $\Delta_{\text{sp}} = (E_0^{N_c+1} + E_0^{N_c-1} - 2E_0^{N_c})/2$  and the excitation gaps  $\Delta_{\text{ex}}^{(n)} = E_n - E_0$  as a function of  $V/t$ . The single-particle gap opens at infinitesimal  $V/t$  and has dip at  $V_c/t$ , while  $\Delta_{\text{ex}}^{(2)}$  closes and reopens at  $V_c/t$ . The inset shows  $\Delta_{\text{ex}}^{(1)}$  is exactly 0 (indicating  $E^\pm$  are exactly degenerate) at  $V < V_c$  and is actually finite (indicating  $A$  and  $B$  are only quasidegenerate) at  $V > V_c$ .

Since the QBCP is the Fermi surface at half-filling, for small size calculations, it is crucial to include the states on the Fermi surface. The Supplemental Material [51] explains in detail the choice of the twisted phases.

*Numerical results.*—Our ED calculations provide the energies of the low-lying eigenstates in the parameter space spanned by  $V/t$  and  $t'/t$ , from which two gapped phases are identified. In each phase, the two lowest lying states are separated from the higher states by a spectral gap. The two lowest lying states in each phase are thus identified as the ground state subspace, from which the symmetry-breaking ground state arises in the thermodynamic limit. As will become clear later, the two gapped phases are distinct as their ground state subspaces have different representations of the  $C_4$  symmetry.

We first present the results for  $t'/t = 1$  for concision. Figure 2(a) shows the low energy spectra as a function of  $V/t$ . At small  $V/t$ , we can see an exact twofold ground state degeneracy, and these two degenerate ground states form the basis of the 2D  $E^\pm$  representation of  $C_4$  point group. This property is actually inherited from the Slater

determinant state in the noninteracting limit. It can be explicitly checked that in the noninteracting limit, the Slater determinants on a finite square lattice with periodic boundary condition (PBC) form  $E^\pm$  of  $C_4$ ; as interaction turns on, the doublet is gapped from the higher states by a finite gap, thus remaining as the same 2D representation. At  $V = V_c \approx 2.81t$ , a level crossing occurs, after which two nearly degenerate excited states become the lowest eigenstates accompanied by the closing and reopening of excitation gap  $\Delta_{\text{ex}}^{(2)}$ , as shown in Fig. 2(b). At  $V > V_c$ , the two states in the ground state subspace belong to the 1D  $A$  and  $B$  representation of  $C_4$ , respectively.

The same holds qualitatively for other values of  $t'/t$ : as  $V$  is turned on, the system immediately enters one gapped phase, referred to as the small- $V$  phase, whose ground state subspace forms the  $E^\pm$  representation of  $C_4$ . Further increasing  $V$ , the system goes through a quantum phase transition and enters another gapped phase, or the large- $V$  phase, whose ground state subspace includes one  $A$  and one  $B$  representation (see Table S1 of Sec. VII in the Supplemental Material [51]). The phase diagram is plotted in Fig. 1(c), where the phase boundary is defined on where the representation of the ground state sector changes (16A) or the avoided level crossing happens (18B, 24D). Having the phase boundaries determined, from here on, we employ our diagnosis scheme to answer the more physical questions: (i) what is the symmetry of the thermodynamic ground state? and (ii) what is the topological number, if any, of the ground state?

We first examine the small- $V$  phase and focus on the 16A cluster, whose ground state sector has two states with  $C_4$  eigenvalues  $+i$  and  $-i$ , denoted by  $E^\pm$ . These two states are exactly degenerate due to time-reversal symmetry, because  $T$  sends a  $C_4$  eigenstate of eigenvalue  $+i$  to another one of eigenvalue  $-i$ . The symmetries of the Hamiltonian,  $T$  and  $C_4$ , may either be preserved or broken in the thermodynamic limit: case (a) the ground state is an eigenstate of  $C_4$ , thus breaking  $T$  and preserving  $C_4$ ; case (b) the ground state is an equal weight superposition of  $E^\pm$ , thus breaking  $C_4$  down to  $C_2$ , and as the two states have the same  $C_2$  eigenvalue  $C_2 = C_4^2 = (\pm i)^2 = -1$ , suggesting a nematic phase.

Now we show that only case (a) is possible for the small- $V$  phase and one can never have a thermodynamic ground state that is a superposition of the  $C_4$  eigenstates with eigenvalues  $\pm i$ . To see this, we first calculate the Chern numbers of the  $C_4$  eigenstates. For a finite system, the Chern number may be defined via its linear response to a twisted phase at the boundaries [52–54]. In Ref. [55], it was shown that, in a weakly interacting system, for any gapped state that is an eigenstate of some rotation operator, its Chern number is directly related to the rotation eigenvalue under periodic boundary condition without twisted phases. Our numerical data suggest that the small- $V$  phase extends to  $V = 0$  and is a gapped phase with weak interaction, so

TABLE I. Symmetry properties of many-body eigenstates of 16A under  $C_4$ . SSB stands for spontaneously symmetry breaking.

Interaction	$\xi(0,0)$	SSB	Chern number
$V < V_c$	$\pm i$	TRS	$\pm 1$
$V > V_c$	$\pm 1$	$C_4 \rightarrow C_2$	0

the Chern number  $C$  is determined by the  $C_4$  eigenvalue  $\xi = 1, -1, i, -i$  up to a multiple of 4

$$i^C = \xi. \quad (2)$$

Using this formula, we determine the Chern numbers of the two lowest lying states  $E^\pm$  as (see Table I).

$$\begin{aligned} C_{E^+} &= 1 \pmod{4}, \\ C_{E^-} &= -1 \pmod{4}. \end{aligned}$$

Next, we argue that the small- $V$  thermodynamic limit ground state cannot be a superposition of  $E^\pm$ . Because if it were the case, since we have just shown  $E^\pm$  have different Chern number, their superposition would imply that the thermodynamic limit ground state has ambiguous Chern number; but this is against the general principle that the ground state of any gapped system should carry a unique Chern number (see Secs. II and III in the Supplemental Material [51] for a detailed discussion). Therefore, the thermodynamic ground state can only be one of  $E^\pm$  with a nonzero Chern number. The small- $V$  phase hence breaks  $T$  and preserves  $C_4$ , and carries a Chern number of  $\pm 1$  up to a multiple of 4. The small- $V$  phase is an interaction-induced QAH state.

For the large- $V$  phase, the two lowest lying states are quasidegenerate: there is a small gap in between that scales with the size of the system to some inverse power. The two states have  $C_4$  eigenvalues of  $+1$  and  $-1$ , respectively, and belong to the 1D  $A$  and  $B$  representation of  $C_4$ . The formula (2) no longer applies in this phase due to the strong interaction. Fortunately, deep in this phase there is a large gap separating the two lowest states from the other part of the spectrum for arbitrary twisted phase (see Fig. 3S in the Supplemental Material [51]); therefore, we can use the winding of the wave function under a different twisted phase to calculate the Chern number, which turns out to be zero for both the  $A$  and  $B$  states. Therefore, any  $C_4$ -breaking local operator may have off-block-diagonal elements in the lowest lying subspace. The thermodynamic ground state is hence a superposition of the two states, which breaks  $C_4$  yet preserves  $C_2$ . Whether or not the thermodynamic ground state breaks  $T$  depends on the relative phase in the coefficients of the superposition. Our ED calculation shows that the matrix elements of the bond current operator are extremely small for large  $V/t$  (not shown). This additional evidence pins down the large- $V$

phase to an NMI, which has zero Chern number. In order for the Chern number to change by an odd integer, a topologically protected level crossing must occur at some special twisted-boundary condition when the system has space-inversion symmetry or higher [54]. That is why we can see a level crossing in the 16A cluster calculation under PBC, as shown in Fig. 2(a).

The above analysis on the ED results help us extract information on the symmetry and the topology of the thermodynamic ground state. It does not, however, give the form of the leading order parameters and the corresponding electronic structures of the phases. To this end, we also perform a mean-field study following Ref. [42], which generates the mean-field phase boundaries in Fig. 1(c). The leading order parameters for the two phases are the current loop and the site nematicity defined as

$$\begin{aligned} m_{\text{QAH}} &= \frac{1}{4} \sum_{\delta=\pm\hat{x},\pm\hat{y}} D_{\delta} \langle \hat{J}_{i,i+\delta} \rangle, \\ m_{\text{NMI}} &= \frac{1}{4} \sum_{\delta=\pm\hat{x},\pm\hat{y}} \langle \hat{\rho}_{i,i+\delta} \rangle, \end{aligned} \quad (3)$$

where  $i$  labels the sites in the  $A$  sublattice and  $D_{\delta} = +1$  for  $\delta = \pm\hat{x}$  and  $-1$  for  $\delta = \pm\hat{y}$ .  $\hat{J}_{i,i+\delta} = i(\hat{c}_i^{\dagger} \hat{c}_{i+\delta} - \hat{c}_{i+\delta}^{\dagger} \hat{c}_i)$  is the current operator.  $\hat{\rho}_{i,i+\delta} = \hat{c}_i^{\dagger} \hat{c}_i - \hat{c}_{i+\delta}^{\dagger} \hat{c}_{i+\delta}$  is the electron density difference between the  $A$  and the  $B$  sublattices. The caricatures of the ordered pattern are shown in the insets of Fig. 1(c).

The mean-field phase diagram is qualitatively consistent with the ED results. However, it fails to predict the insulating behavior of NMI when the site-nematic order parameter is small (see Sec. VI in the Supplemental Material [51]). Also we note that the ED results show a larger area of the QAH phase, indicating an overestimate of the site-nematic order in the mean-field calculations. More importantly, we also computed the correlation functions of the order parameters in ED,

$$\begin{aligned} S_{\text{QAH}} &= \frac{1}{4} \sum_{i \in A} \sum_{\delta} D_{\delta} \langle \hat{J}_{i,i+\delta} \hat{J}_{i_0,i_0+\delta_0} \rangle, \\ S_{\text{NMI}} &= \frac{1}{4} \sum_{i \in A} \sum_{\delta} \langle \hat{\rho}_{i,i+\delta} \hat{\rho}_{i_0,i_0+\delta_0} \rangle, \end{aligned} \quad (4)$$

where we have used the translation symmetry and  $i_0, i_0 + \delta_0$  is the reference bond. For comparison, here we present the results along the line  $t = t'$  and plot the correlation functions versus  $V/t$  in Fig. 3. At small  $V/t$ , the broad peak in the QAH current loop structure factor [see Fig. 3(a)] signifies that the QAH phase will be stable in the thermodynamic limit. The possibility of a bond-nematic phase in the small  $V/t$  is also considered, but its correlation is clearly short ranged (see Sec. V in the Supplemental Material [51]). At large  $V/t$ ,  $S_{\text{NMI}}$  quickly increases and

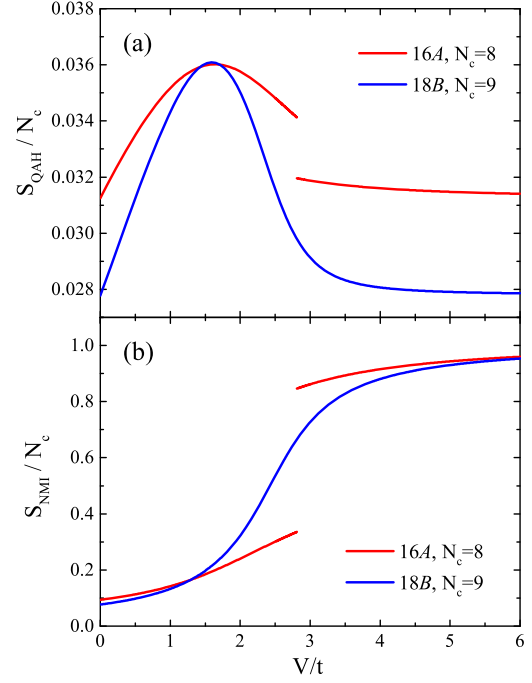


FIG. 3. The structure factors of the (a) QAH and (b) NMI phases. The discontinuity in the 16A results is due to the level crossing. We clearly see the enhancement of the QAH structure factor at  $V < V_c$  and the saturation of the NMI structure factor at  $V > V_c$ .

it saturates at  $S_{\text{NMI}} = 1$  in the  $V/t \rightarrow \infty$  [see Fig. 3(b)], indicating that all electrons are located at either  $A$  sites or  $B$  sites.

*Discussion.*—Finally, we discuss the transition between the small- $V$  QAH and the large- $V$  NMI phases. The QAH phase preserves  $C_4$  and breaks  $T$ , while the NMI phase breaks  $C_4$  and preserves  $T$ . Therefore, they can either be separated by a first-order transition line or a region of the coexisting phase (breaking both  $T$  and  $C_4$ ). In the mean-field calculation (see Fig. 1 or in Ref. [42]), there is a very small region where both order parameters are nonvanishing, while the data from ED are insufficient to draw any conclusion. We conjecture there is a first-order transition. If there were a coexisting phase, the thermodynamic ground state presumably arises from the joint ground state subspaces of QAH and NMI, i.e., a linear superposition of the  $E^{\pm}$  representation and the  $A$  and  $B$  representations of  $C_4$ . But we know that due to the difference in Chern numbers, only the  $A$  and  $B$  representations, both having vanishing Chern number, can be linearly superimposed. In other words, the thermodynamic ground state cannot have a finite Chern number while being a superposition of different representations of  $C_4$ , so the QAH phase must preserve  $C_4$  and cannot coexist with the NMI phase.

We would like to thank Zheng-Xin Liu and Lei Wang for helpful discussion. H. Q. W. would like to thank Rong-Qiang He for helpful discussions about the Lanczos exact diagonalization method. Z. Y. M. is particularly indebted to

D. Wang and H. Fan for their early engagement and stimulating discussions that motivate this study. The numerical calculations were carried out at the Physical Laboratory of High Performance Computing in RUC as well as the National Supercomputer Center in Guangzhou on the Tianhe-2 platform. C. F. and Z. Y. M. acknowledge support from the Ministry of Science and Technology (MOST) of China under Grants No. 2016YFA0302400 and No. 2016YFA0300502. H. Q. W., Y. Y. H., Z. Y. M., and Z. Y. L. acknowledge support from the National Natural Science Foundation of China (NSFC) under Grants No. 11474356, No. 91421304, No. 11421092, and No. 11574359. C. F. and Z. Y. M. are also supported by the National Thousand-Young-Talents Program of China.

*Note added.*—We have recently become aware of an interesting work [56] where the interaction-driven spontaneous quantum Hall effect is observed on a kagome lattice via ED and DMRG.

\*cfang@iphy.ac.cn

†zymeng@iphy.ac.cn

- [1] C. Wu and S.-C. Zhang, *Phys. Rev. Lett.* **93**, 036403 (2004).  
 [2] J. Wen, A. Rüegg, C.-C. Joseph Wang, and G. A. Fiete, *Phys. Rev. B* **82**, 075125 (2010).  
 [3] D. A. Pesin and L. Balents, *Nat. Phys.* **6**, 376 (2010).  
 [4] E. V. Castro, A. G. Grushin, B. Valenzuela, M. A. H. Vozmediano, A. Cortijo, and F. de Juan, *Phys. Rev. Lett.* **107**, 106402 (2011).  
 [5] C. Xu, *Phys. Rev. B* **83**, 024408 (2011).  
 [6] K.-Y. Yang, W. Zhu, D. Xiao, S. Okamoto, Z. Wang, and Y. Ran, *Phys. Rev. B* **84**, 201104 (2011).  
 [7] M. Kurita, Y. Yamaji, and M. Imada, *J. Phys. Soc. Jpn.* **80**, 044708 (2011).  
 [8] K. Sun, W. V. Liu, A. Hemmerich, and S. Das Sarma, *Nat. Phys.* **8**, 67 (2012).  
 [9] J. W. F. Venderbos, S. Kourtis, J. van den Brink, and M. Daghofer, *Phys. Rev. Lett.* **108**, 126405 (2012).  
 [10] Z. Xu and S. Chen, *Phys. Rev. B* **88**, 045110 (2013).  
 [11] B. Dóra, I. F. Herbut, and R. Moessner, *Phys. Rev. B* **90**, 045310 (2014).  
 [12] I. F. Herbut and L. Janssen, *Phys. Rev. Lett.* **113**, 106401 (2014).  
 [13] M. Imada, Y. Yamaji, and M. Kurita, *J. Phys. Soc. Jpn.* **83**, 061017 (2014).  
 [14] S. Kitamura, N. Tsuji, and H. Aoki, *Phys. Rev. Lett.* **115**, 045304 (2015).  
 [15] Y. Wang, Z. Wang, Z. Fang, and X. Dai, *Phys. Rev. B* **91**, 125139 (2015).  
 [16] J. Maciejko and G. A. Fiete, *Nat. Phys.* **11**, 385 (2015).  
 [17] T. Kondo, M. Nakayama, R. Chen, J. J. Ishikawa, E.-G. Moon, T. Yamamoto, Y. Ota, W. Malaeb, H. Kanai, Y. Nakashima, Y. Ishida, R. Yoshida, H. Yamamoto, M. Matsunami, S. Kimura, N. Inami, K. Ono, H. Kumigashira, S. Nakatsuji, L. Balents, and S. Shin, *Nat. Commun.* **6**, 10042 (2015).  
 [18] J. W. F. Venderbos and L. Fu, *arXiv:1506.05479*.  
 [19] S. Raghu, X.-L. Qi, C. Honerkamp, and S.-C. Zhang, *Phys. Rev. Lett.* **100**, 156401 (2008).  
 [20] C. Weeks and M. Franz, *Phys. Rev. B* **81**, 085105 (2010).  
 [21] N. A. García-Martínez, A. G. Grushin, T. Neupert, B. Valenzuela, and E. V. Castro, *Phys. Rev. B* **88**, 245123 (2013).  
 [22] Y. Jia, H. Guo, Z. Chen, S.-Q. Shen, and S. Feng, *Phys. Rev. B* **88**, 075101 (2013).  
 [23] S. Goto, K. Masuda, and S. Kurihara, *Phys. Rev. B* **90**, 075102 (2014).  
 [24] M. Daghofer and M. Hohenadler, *Phys. Rev. B* **89**, 035103 (2014).  
 [25] H. Guo and Y. Jia, *J. Phys. Condens. Matter* **26**, 475601 (2014).  
 [26] J. Motruk, A. G. Grushin, F. de Juan, and F. Pollmann, *Phys. Rev. B* **92**, 085147 (2015).  
 [27] S. Capponi and A. M. Läuchli, *Phys. Rev. B* **92**, 085146 (2015).  
 [28] D. D. Scherer, M. M. Scherer, and C. Honerkamp, *Phys. Rev. B* **92**, 155137 (2015).  
 [29] F. Zhang, J. Jung, G. A. Fiete, Q. Niu, and A. H. MacDonald, *Phys. Rev. Lett.* **106**, 156801 (2011).  
 [30] A. Rüegg and G. A. Fiete, *Phys. Rev. B* **84**, 201103 (2011).  
 [31] T. Pereg-Barnea and G. Refael, *Phys. Rev. B* **85**, 075127 (2012).  
 [32] T. Yoshida, R. Peters, S. Fujimoto, and N. Kawakami, *Phys. Rev. Lett.* **112**, 196404 (2014).  
 [33] S. Jiang, A. Mesáros, and Y. Ran, *Phys. Rev. X* **4**, 031040 (2014).  
 [34] S. Jiang and Y. Ran, *Phys. Rev. B* **92**, 104414 (2015).  
 [35] M. Kurita, Y. Yamaji, and M. Imada, *arXiv:1511.02532*.  
 [36] W. Zhu, S. S. Gong, and D. N. Sheng, *arXiv:1509.05509*.  
 [37] M. Golor and S. Wessel, *Phys. Rev. B* **92**, 195154 (2015).  
 [38] J. W. F. Venderbos, M. Manzardo, D. V. Efremov, J. van den Brink, and C. Ortix, *Phys. Rev. B* **93**, 045428 (2016).  
 [39] Z. Wang, Y. D. Chong, J. D. Joannopoulos, and M. Soljačić, *Phys. Rev. Lett.* **100**, 013905 (2008).  
 [40] Y. D. Chong, X.-G. Wen, and M. Soljačić, *Phys. Rev. B* **77**, 235125 (2008).  
 [41] K. Sun and E. Fradkin, *Phys. Rev. B* **78**, 245122 (2008).  
 [42] K. Sun, H. Yao, E. Fradkin, and S. A. Kivelson, *Phys. Rev. Lett.* **103**, 046811 (2009).  
 [43] S. Uebelacker and C. Honerkamp, *Phys. Rev. B* **84**, 205122 (2011).  
 [44] J. M. Murray and O. Vafek, *Phys. Rev. B* **89**, 201110 (2014).  
 [45] V. L. Ginzburg, *Sov. Phys. Solid State* **2**, 1824 (1960).  
 [46] The possible interaction-driven topological phases have also been studied on other 2D lattices with QBCP, like kagome lattice [2,47], Lieb lattice [48,49], and honeycomb lattice [35,38].  
 [47] Q. Liu, H. Yao, and T. Ma, *Phys. Rev. B* **82**, 045102 (2010).  
 [48] W.-F. Tsai, C. Fang, H. Yao, and J. Hu, *New J. Phys.* **17**, 055016 (2015).  
 [49] M. M. A. Dauphin and M. A. Martin-Delgado, *arXiv:1510.00281*.  
 [50] J.-M. Hou, *Phys. Rev. Lett.* **111**, 130403 (2013).  
 [51] See Supplemental Material at <http://link.aps.org/supplemental/10.1103/PhysRevLett.117.066403> for details about the cluster geometries in the ED calculations, the

- twisted phases at the boundary for each cluster, the finite-size scaling of the single-particle gap, and the measurements of the bond nematic structure factor.
- [52] Q. Niu, D. J. Thouless, and Y.-S. Wu, *Phys. Rev. B* **31**, 3372 (1985).
- [53] T. Fukui, Y. Hatsugai, and H. Suzuki, *J. Phys. Soc. Jpn.* **74**, 1674 (2005).
- [54] C. N. Varney, K. Sun, M. Rigol, and V. Galitski, *Phys. Rev. B* **84**, 241105 (2011).
- [55] C. Fang, M. J. Gilbert, and B. A. Bernevig, *Phys. Rev. B* **86**, 115112 (2012).
- [56] W. Zhu, S. S. Gong, T. S. Zeng, L. Fu, and D. N. Sheng, [arXiv:1604.07512](https://arxiv.org/abs/1604.07512).